Practical implementation and remaining problems for the film linearized muffin-tin orbital calculation of surface electronic structure

Cheng-Quinn Ma,* M. V. Ramana,† and Bernard R. Cooper
Department of Physics, West Virginia University, Morgantown, West Virginia 26506

H. Krakauer
Department of Physics, College of William and Mary, Williamsburg, Virginia 23185
(Received 23 September 1985)

We describe the details of implementation of the film linearized muffin-tin orbital method of Krakauer and Cooper [Phys. Rev. B **16**, 605 (1977)] for slab geometries. Using the constrained wave functions as described by Krakauer and Cooper, we get consistently good results except for the work function. We describe an alternate method that we have also implemented to improve the work function. This discards the plane-wave orbitals while striving to improve the quality of the basis functions for describing the vacuum behavior without increase in matrix sizes. We find the quality of results poorer; therefore, in Appendix A, we suggest a way of increasing the variational freedom by removing the constraint on the plane-wave orbitals. We report on our investigations on the stability of the results with respect to variations in the most sensitive energy parameters that appear in the theory, and the effect on the results of various shaping approximations on the charge density and on the potential. We find that because of the small matrix sizes, diagonalization times are an insignificant portion of the total running time for a complete iteration. This total time per iteration is only slightly faster (by a factor of 1.6) than a corresponding linearized augmented-plane-wave iteration. However, because the small matrix sizes imply memory requirements which are smaller than those of other methods currently in use, systems with a greater number of atoms in the unit cell may be studied (for a given computer) than with those methods.

I. INTRODUCTION

A device widely used to calculate electronic structure of transition- and noble-metal surfaces, and such surfaces with chemisorbed species, is to use a slab geometry. This device is based on the fact that the "healing length" for d-band metals is rather short, and so for a five-layer system the center layer exhibits close to bulklike behavior. Thus the surface of the slab provides a good representation for the surface of a bulk metal. The semi-infinite system, with an infinite number of atoms in a two-dimensional unit cell is replaced by a system finite in the direction perpendicular to the surface with a finite number N of atoms in the unit cell. If there are N_L layers in the slab with N_A atoms per layer then $N=N_L N_A$. Systems with layers of one metal on a substrate of another, with chemisorption at the surface of the former, involve a slab of many layers. This arises out of the requirement that regions far from the interface exhibit bulklike behavior; while compounds, lower-symmetry solids, and relatively dilute chemisorption superlattices involve large two-dimensional unit cells with many atoms per layer. The number of atoms per unit cell is, therefore, typically much larger than for bulk systems. The large number of atoms and the requirement of self-consistency, means long computer running times and large computer memory requirements. The kinds of physical systems, with surfaces of interest, that may be studied using slab geometries are limited by the available computer resources. This, for example, limits the utility of the highly productive linearized augmented-plane-wave (LAPW) technique[1,2] for treating complex systems as described above. This is because of the relatively large number of augmented-plane waves (APW's) per atom, typically 50 or 60 for transition metals, necessary to accurately represent the behavior. Examples of calculations that encounter such limitations are a recent LAPW calculation[3] with 12 atoms per unit cell that required a Cray computer, and a localized (Gaussian) orbital calculation[4] for 11 layers of Ti(0001) that resorted to approximate self-consistency to avoid a fully-self-consistent calculation involving a 206×206 secular determinant. (The corresponding LAPW determinant would be about 3 times as large.) Our film linearized muffin-tin orbital (FLMTO) method, to be described below, would require a 99×99 secular determinant for this case.

The attractiveness of a method that would require relatively smaller running times and memory requirements, without sacrificing ability to investigate physical systems with a large number of atoms in the unit cell, has strongly motivated us to fully implement the FLMTO method (involving a linearized combination (LC) of muffin-tin orbitals (MTO's) and plane-wave orbitals (PWO's) [LC(MTO-PWO)] described in the earlier work of Krakauer and Cooper[5] (referred to as KC in the rest of the paper). For example, we want to study such large-scale surface problems as the effect[6] of copper monolayer, and submonolayer coverages, on the chemisorption of carbon monoxide on transition metals.[7] The value of the linearized muffin-tin orbital (LMTO) technique in bulk

calculations[8,9] has been well demonstrated. For example, Jarlborg *et al.*[10] have used this technique for calculations on ternary compounds such as YRh_4B_4. This involved 18 atoms per unit cell. Use of a maximum value of l of 1 (4 basis functions) for the 8 boron atoms and of 2 (9 basis functions) for the other 10 atoms led to a 122×122 secular determinant.

This paper is a report on the progress of our efforts to keep computer time and memory requirements small and yet ensure adequate quality of results to capture the physics of the systems we will study. We evaluate our results by a comparison of our layer-projected density of states with other high-quality calculations, and of our work functions with experimental values. Good values for these two quantities, we hope, will ensure good charge densities and detailed-band structures. The question of such comparison has recently been discussed in detail by Jepsen and Wilkins.[11]

Our efforts at minimizing computer requirements, briefly, consisted of using an absolutely minimal basis set obtained by constraining the vacuum functions by the vacuum "tail cancellation condition" as outlined in KC, and of trying various shaping approximations for the potential. Using the same input muffin-tin (MT) potential, for five-layer (100) copper, our LC(MTO-PWO) calculation only needs a 45×45 secular determinant to show agreement in energy eigenvalues (after a single diagonalization) with a corresponding LAPW calculation, to within one millirydberg (mRy) in the region of the d bands. However, while the diagonalization time is 120 times smaller, a complete iteration consisting of a sequential solution of the Schrödinger and Poisson equations is only 1.6 times as fast for a potential that is completely general in all regions except the MT. Almost all the time saved in diagonalization is lost in the setup of the secular determinant. Even this time advantage may be lost with our anticipated increase in variational freedom outlined in the Appendix. However, our secular determinant size increases much more slowly with increasing number of atoms in the unit cell, so that we anticipate a substantial advantage in being able to study the large systems of interest mentioned in the beginning of this section. Other methods that also can require only a small basis are the linear combination of atomic orbitals (LCAO) method, and the recently suggested linear augmented Slater-type orbital method[12] (LASTO). In the next section we describe the LC(MTO-PWO) method and our experience with it, which motivates a variant of this method. We call this variant the linearized augmented muffin-tin orbital (LAMTO) method, and give a brief description of it.

To complete this introduction we make some remarks about our calculations to put them into perspective with respect to other slab geometry calculations. We do not make use of the atomic-sphere approximation (ASA). The core states in our calculations are allowed to relax at each iteration, i.e., they are recalculated for the new potential at each iteration; we therefore can calculate core-level shifts. In addition, our wave functions in the vacuum region are given in the Laue representation (i.e., the wave functions are expressed in basis functions given as the product of a plane-wave factor, giving the dependence parallel to the surface, times a numerically determined factor, giving the dependence normal to the surface, which has the correct exponential decay for substantial distances outside the surface). This means that the LC(MTO-PWO) technique is an appropriate one for calculating[13] the surface-He (or other) atom interaction potential for use in understanding monoenergetic atomic beam diffraction from single-crystal surfaces. As is generally done at the present time, we treat the exchange and correlation potential in the local-density approximation using density functional theory.[14] We use the Wigner[15] interpolation scheme for the evaluation of the correlation potential.

In this paper we present a systematic investigation of several important aspects of the implementation of linear band theory using the self-consistent LMTO technique for thin-film (slab) geometry. We first exhibit the close agreement of LC(MTO-PWO) and LAPW eigenvalues (non-self-consistent) for the same input potential. Next, we study the effect of varying the energy parameters involved in the linearization (i.e., values of fixed energy chosen for calculating the basis functions) on the band-energy eigenvalues and on the work function, and thereby characterize the degree of intrinsic uncertainty introduced into the self-consistently-determined band structure through the linearization procedure. We then study the effect of including various degrees of complexity in the shape approximations used to treat the charge density as input to the Poisson equation and the potential as input to the Schrödinger equation. Finally, where appropriate, we report the corresponding results with the LAMTO method. We characterize the quality of self-consistent results through comparison with the experimental work function and with layer density of states (LDOS) from other calculations for $\langle 100\rangle$ copper (our test case).

In discussing the benefits and limitations of the LC(MTO-PWO) technique we will use calculations employing the surface linear augmented plane wave (LAPW) technique[1,2] as a basis for comparison since both these techniques construct their basis functions using a film muffin-tin potential,[5] as well as both being based on variational principles in energy.

Our aim has been systematically to develop the FLMTO method and thereby to gain the advantages of an LMTO-type methodology for studies of surface electronic structure. In Sec. II we present an overview of our experiences with the implementation of the LMTO method for slabs for both the LC(MTO-PW) and the LAMTO method; we follow this with Sec. III on methodology. In Sec. IV we present and discuss our results in detail for both methods and fully motivate Appendix A where we outline a way to generalize the LC(MTO-PWO) method to be able to use independent functions in the vacuum. In the final section we summarize the status of the self-consistent FLMTO method, and discuss some criteria for defining success in the development of such a self-consistent method for calculating surface electronic structure.

This paper is a progress report on our attempts to implement efficiently the self-consistent LMTO technique as applied to surfaces with the strong objective of keeping

the basis size absolutely minimal throughout our various efforts.

II. AN OVERVIEW OF OUR IMPLEMENTATION OF THE LMTO METHOD FOR SLAB GEOMETRY

The central feature of the LC(MTO-PWO) method[5] is the introduction of a basis consisting of (a) MT orbitals (MTO's) to treat the region within the nominal film boundaries and (b) additional functions which we call "plane-wave-orbitals" (PWO's), which are constructed from the exact solutions of the Schrödinger equation in the regions exterior to the film (i.e., "the vacuum"), and which are used to treat the vacuum behavior. The great advantage of the LMTO technique is that one deals with a small basis of functions to represent the electronic behavior. This advantage is shared with its "parent" Korringa-Kohn-Rostoker (KKR) technique.[16] However, the fact that the muffin-tin orbital technique is based on a variational principle, with the variation being in energy, permits linearization, i.e., neglect of the energy dependence of the basis MTO and PWO functions over a certain energy range, thereby giving energy-independent Hamiltonian and overlap matrix elements, and hence a secular determinant that is linear in energy. With an appropriate choice of energy parameters (e.g., specification of E values for $l=0,1,2$ and vacuum, and a value of κ specifying the kinetic energy) for use in the equations defining the MTO and PWO functions [see Eqs. (4) and (5) of Ref. 6], the eigenvalues (band and surface-state energies) of the system can be determined accurately over a large energy range by a simple diagonalization of the secular determinant. Thus one has the advantage of a small energy-independent basis without the disadvantage of having to calculate energy-dependent lattice sums. Also, since it is a local orbital basis, it offers better ease in physical interpretation (visualization in terms of scattering of electrons off core sites) than plane-wave-type methods such as APW.

We now turn to practical questions of efficient implementation of the LC(MTO-PWO) method without sacrifice in quality of results. We have tried to maximize the efficiency of the method by minimizing the size of the basis set, and by experimenting with various shaping approximations of the potential. *To minimize the number of basis functions, the basis set was constrained by imposing a tail-cancellation condition in the vacuum, as described in* KC, *thus eliminating independent functions from the vacuum region.* This is done by first expressing the wave function as[5] a linear combination of MTO's $[\chi_{\alpha,L}(\mathbf{r}-\mathbf{R})]$ centered at the various atomic sites spanned by $\mathbf{R}$, the two-dimensional direct-lattice vector, and of PWO's corresponding to the upper and lower vacuum regions $[\chi_{1,m}(\mathbf{r})$ and $\chi_{2,m}(\mathbf{r})]$,

$$\Psi_{\mathbf{k}}(\mathbf{r})=\sum_{\alpha,L}A_{\alpha,L}\sum_{\mathbf{R}}e^{i\mathbf{k}\cdot\mathbf{R}}\chi_{\alpha,L}(\mathbf{r}-\mathbf{R}) + \sum_{m}[A_{1,m}\chi_{1,m}(\mathbf{r})+A_{2,m}\chi_{2,m}(\mathbf{r})]\ . \tag{2.1}$$

To decrease the number of independent coefficients in the variational calculation, the tail-cancellation condition is used to express the $A_{1,m}$ and $A_{2,m}$, the coefficients for the upper and lower vacuum PWO's, in terms of the $A_{\alpha,L}$, the MTO coefficients. For d-transition element atoms, this has the practical effect of reducing the size of the basis set to 9 basis functions ($l=0,1,2$) per atom. We note that with this procedure the tails of the vacuum PWO's are still present in the MT sphere and interstitial regions. As will be discussed in Sec. IV on results, their presence may be important for ensuring adequate quality of the basis functions.

As already noted, with this vacuum tail-cancellation constraint, for d-band metals we have 9 independent functions per atom. This is only about one-sixth as many as in the LAPW method. Our secular determinant and the diagonalization time is correspondingly much smaller, being about 120 times faster for five-layer ⟨100⟩ copper. The actual running time for one complete iteration (sequential solution of Schrödinger and Poisson equations) depends on the method used to calculate contributions from the interstitial to the Hamiltonian and overlap matrix elements and the degree of spatial variation allowed in the potential in each region. Allowing full spatial variation in the potential in the interstitial and vacuum regions and using the fast Fourier transform (FFT) method leaves the LC(MTO-PWO) method with a time advantage of a factor of 1.6 for five-layer ⟨100⟩ copper. Almost all the advantage gained in diagonalization of the small secular determinant is lost in the calculation of contributions from the interstitial to the Hamiltonian matrix arising from full spatial variation of the interstitital potential. This loss of running time in the setup of the Hamiltonian matrix has two sources. One is that the nature of the LC(MTO-PWO) basis functions requires the use of complex arithmetic with a single complex multiplication taking up as much time as four real multiplications. The second is that the solution of the Poisson equation for the interstitial region is in the plane-wave form so that the calculation of the Hamiltonian matrix elements involves a time-consuming three-dimensional double Fourier sum. We use the less time-consuming alternative of transforming the potential and basis functions to real space with the FFT and carrying out the integrations in real space. We also use the FFT for charge density synthesis and for the calculation of the exchange-correlation contribution to the potential in the interstitital region. We now briefly report our results with the LC(MTO-PWO) method beginning with some discussion of work reported earlier.[17]

The results reported in Ref. 17 were with a potential that was planar averaged in the interstitial and vacuum regions over planes parallel to the film (i.e., that included "vertical warping"). The reported time advantage of a factor of 3 over the corresponding LAPW calculation was with a one-dimensional double Fourier sum for the vertical warping contribution to the Hamiltonian matrix elements from the interstitital region. This planar-averaged (vertically-warped) potential in the interstitial region gave us work functions in excellent agreement with experiment for five-layer ⟨100⟩ copper and nickel and layer density of states comparable to other calculations, and layer density of states for five-layer ⟨0001⟩ ruthenium that we judged to be good. The work function for ruthenium,

however, was disappointingly too small (by about 1 eV) compared to the experimental[18] value. We therefore implemented the FFT to handle potentials of more general spatial variation (full warping) in the interstitial region and included code to handle full warping in the vacuum. With the fully-warped potential (except in the muffin-tin region) the work function for five-layer ⟨100⟩ copper becomes too large, by about 1.5 eV. The layer density of states did not change in any significant way as far as we could judge by simply looking at the plots corresponding to the vertically- and fully-warped cases. This behavior of the work function for five-layer ⟨100⟩ copper is difficult to understand. The good agreement with experiment for copper and nickel with the vertically-warped potential may be due to the procedure used for planar averaging the potential in the interstitital region. The method used for planar averaging is not unique because of the presence of the MT holes. The details of this will be discussed in Sec. IV. However, no ambiguity in the potential exists for the fully-warped result.

Thus we were led to conclude that there is a fundamental problem in calculating reliable work functions with the LC(MTO-PWO) method. We feel that the origins of this difficulty lie in the use of the tail-cancellation condition. Since the vacuum functions are restricted by the tail-cancellation condition, we believe that this unduly constrains the behavior of the charge in the surface region to which the work function is sensitive. To release this constraint without increasing the number of basis functions we tried the LAMTO method outlined below.

The LAMTO basis functions use the same MTO's as the LC(MTO-PWO) method. The important difference from the latter method is that the PWO's are discarded and at the vacuum boundary a linear combination of u_m and $\dot{u}_m$ ("dot" means energy derivative)—the solution and its energy derivative, of the Schrödinger equation in the vacuum region—is matched with continuous logarithmic derivative to a lattice sum of MTO's at the nominal boundary (because of the imposed tail-cancellation condition in vacuum, $\dot{u}_m$ does not appear in our original FLMTO methodology). (The LAMTO method that we developed and implemented[19] *seems* to be identical, insofar as we can judge, to that used in recently published work by Kasowski and Tsai.[20]) With this basis the layer density of states for five-layer ⟨100⟩ copper is quite poor, especially for the surface layer (compared to other calculations[21,22] which agree among themselves), while the work function is sensitive to the exact details of the MTO's (i.e., choice of energy parameters E_l and choice between use of Hankel and Neumann functions, see Ref. 23) that are used, and can vary by as much as 2 eV. The LAMTO method is unsatisfactory without further improvements in variational quality. Unlike the LC(MTO-PWO) method, it does not reduce to the film KKR method in the exact limit; and it is therefore difficult to see the directions in which the method may be systematically improved.

In those cases where we could compare to results of other calculations,[21,22,24] the LC(MTO-PWO) method gave us good results, except for the work function,[18,21,22,24] even when we only used vertical warping. We therefore feel it more useful to improve the LC(MTO-PWO) method by dropping the variational constraint of tail cancellation in the vacuum than to pursue the LAMTO method. Using the methodology outlined in Appendix A, a modest increase in basis size should retain the essential advantages of the method and give good work functions. As discussed in Sec. III on methodology and in the concluding remarks of Sec. V, this increase in basis size giving independent PWO basis functions would relieve the constraint on the charge density behavior in the vacuum boundary region, which is the probable cause of the problems with the work function, essentially without modifying the spectral density relative to the Fermi energy. For a five-layer copper system the running time for the method of Appendix A should be about the same as for an LAPW calculation for a five-layer copper system. For larger systems the basis size would not increase as fast as for the LAPW method since the number of site-centered functions remains the same (9 per atom for *d*-band metals) and we do not foresee the need for increasing the number of independent PWO's.

III. METHODOLOGY

In this section we present the details of our methodology and some techniques of implementation. In Sec. III A we outline the choice of our basis functions and in Sec. III B we write down the wave function in each region of space for the LC(MTO-PWO) method. In Sec. III C the wave functions for the LAMTO method are given. The solution of the Poisson equation is discussed in Sec. III D and the various shaping approximations for the charge and the potential are discussed. The setup of the secular determinant is presented in Sec. III E.

A. Basis functions: Linearization and core orthogonalization

The basis functions are defined with respect to the film muffin-tin potential with the geometry shown in Fig. 1. The film muffin-tin-potential is angular averaged in the muffin-tin sphere, region I; volume averaged in the interstitial, region II; and planar-averaged parallel to the plane of the film, in the vacuum extending from $\pm z_1$ to $\pm\infty$, respectively, region III. This film muffin-tin potential is recalculated at each iteration, and we emphasize that this restricted form of the potential is only used in defining the basis functions (as in the LAPW method). A more general form of the potential can then be used in solving the secular equation through the application of a variational principle. We use the MTO and PWO basis functions, given by Eqs. (4), (8), and (A1) of KC with one modification (outlined in Sec. V of KC). The modification is to replace J_l and K_l in Eq. (4a) of KC, i.e., to modify the definition of the MTO's and PWO's in the MT sphere regions. J_l is replaced by $\tilde{J}_l$ which is a linear combination of $u_{\alpha,l}$ and $\dot{u}_{\alpha,l}$, where $\dot{u}_{\alpha,l}$ is the energy derivative[8] of $u_{\alpha,l}$. (Here, as in KC, $u_{\alpha,l}$ is the solution of the Schrödinger equation for the αth muffin-tin spherical potential part of the film muffin-tin potential and is normalized to unity in the MT sphere region.) Thus

$$\tilde{J}_l = \dot{s}_l u_{\alpha,l} - s_l \dot{u}_{\alpha,l} \ . \tag{3.1a}$$

Then for $\mathbf{r}' = \mathbf{r} - \tau_\alpha$ in the αth MT sphere

$$\chi_{\alpha,l}(\mathbf{r}') = i^l Y_L(\mathbf{r}')[a_{\alpha,l} u_{\alpha,l}(r') + b_{\alpha,l} \dot{u}_{\alpha,l}(r')] \ , \quad |\mathbf{r}'| \le S_\alpha \ , \tag{3.1b}$$

where $L = \{l,m\}$, $\dot{u}_{\alpha,l} = [\partial u_{\alpha,l}/\partial E]_{E=E_l}$, S_α denotes the αth muffin-tin sphere radius and E_l is the energy parameter chosen to represent bands of a given l character. The coefficients in Eqs. (3.1a) and (3.1b) are determined by the continuity conditions on the MTO basis functions and their radial derivatives at the muffin-tin sphere radius.

This replacement of J_l by $\tilde{J}_l$ has the desirable feature of supplying the first correction term in the linearized energy-independent basis functions and at the same time guarantees orthogonalization[25] to the core functions at all sites $\alpha \neq \beta$ as well as for $\alpha = \beta$. Since Eq. (3.1) changes the definition of the αth MTO within the αth MT sphere, the definition of K_l in Eq. (4c) of KC for the αth MTO outside the αth muffin-tin sphere must also be changed. This is done by replacing K_l with $\tilde{K}_l$ given by Eq. (24) of KC when J_l is replaced by $\tilde{J}_l$. This gives

$$\chi_{\alpha,L}(\mathbf{r}) = s_l \tilde{K}_{\alpha,L}(\kappa,\mathbf{r})$$

and

$$\tilde{K}_{\alpha,L}(\mathbf{r}) = 4\pi \sum_{L',L''} C_{LL'L''} \kappa^{l+l'-l''} \tilde{J}_{L'}(\kappa, \mathbf{r} - \mathbf{R} - \tau_\beta) \times K^*_{L''}(-\mathbf{R} - \tau_\beta + \tau_\alpha) \tag{3.2a}$$

when $\mathbf{r}$ is within all other MT spheres; and

$$\tilde{K}_{\alpha,L}(\mathbf{r}') = i^l Y_L(\mathbf{r}')(i\kappa^{l+1}) h_l^{(1)}(\kappa r') \tag{3.2b}$$

when $\mathbf{r}$ is in the interstitial, i.e., neither in any muffin-tin sphere nor in the vacuum. Note that in the interstitial region $\tilde{K}_{\alpha,L}(\mathbf{r}) = K_{\alpha,L}(\mathbf{r})$. The PWO's for $\mathbf{r}$ within the MT spheres is given by Eq. (25) of KC.

Before closing this subsection, we define another set of functions in the MT sphere regions. To calculate the interstitital contribution to the Hamiltonian and overlap matrices and to solve the Poisson equation in the interstitial region, we have to deal with an awkward geometrical shape consisting of a parallelopiped with spherical holes in it. We deal with this geometry by extending the interstitial functions into the holes by choosing "pseudo-muffin-tin" functions which have the form appropriate to the MT sphere with zero potential:

$$\tilde{\chi}_{\alpha,L}(\mathbf{r}') = i^l Y_l(\mathbf{r}')[c_{\alpha,l} r'^l + d_{\alpha,l} r'^{l+2}], \quad |r'| < S_\alpha \ , \tag{3.3}$$

where $c_{\alpha,l}$ and $d_{\alpha,l}$ are determined by continuity at the MT sphere boundary with the true interstitial functions of Eq. (4a) of KC.

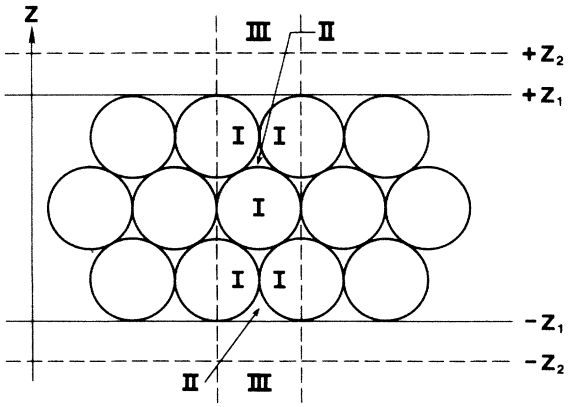

FIG. 1. Schematic figure showing geometry used to define the film muffin-tin potential. Regions I, II, and III and boundaries at $\pm z_1$ and $\pm z_2$ are described in the text.

B. Wave functions in the three regions

We follow the Appendix of KC for writing the wave function in the three regions shown in Fig. 1. Starting from the film wave function [Eq. (A1) of KC] and using the vacuum tail-cancellation conditions [Eqs. (A3a) and (A3b) of KC] to eliminate the A_{im} coefficients, we arrive at Eq. (A5a) of KC which we no longer require to be zero. Substituting Eq. (A5a) of KC in Eq. (A1) of KC we have the generalizations of Eqs. (20a) and (20b) of KC for multilayer films for $\kappa^2 > 0$.

The representation of the linearized film wave function for $\mathbf{r}$ in the βth muffin-tin sphere region is

$$\Psi^b_{\mathbf{k}}(\mathbf{r}) = \sum_{\alpha,L} A^b_{\alpha,L}(\mathbf{k}) \left[\Phi_L(N^\alpha_l, \mathbf{r}')\delta_{\alpha\beta} + \sum_{L'} \frac{\Phi_{L'}(J^\beta_{l'}, \mathbf{r}')}{\omega_{l'}(N^\beta_{l'}) - \omega_{l'}(J^\beta_{l'})} \Delta^{\beta\alpha}_{L'L} \right], \quad |\mathbf{r}'| \le S_\beta \tag{3.4}$$

where $\mathbf{r}' = \mathbf{r} - \tau_\beta$. The structure matrix $\Delta^{\beta\alpha}_{L'L}$ includes the effect of all off-site basis function "tails." Other quantities in (3.4) are defined as follows:

$$\Phi_L(f^\beta_l, \mathbf{r}') \equiv i^l Y_L(\mathbf{r}')[u_{\beta,l}(r) + \omega_l(f^\beta_l)\dot{u}_{\beta,l}(r')] \ , \tag{3.5a}$$

$$\omega_l(f^\beta_l) \equiv -\frac{u^\beta_l D(f^\beta_l) - D(u^\beta_l)}{\dot{u}^\beta_l D(f^\beta_l) - D(u^\beta_l)} \ , \tag{3.5b}$$

where

$$D(f^\beta_l) \equiv S_\beta [(f^\beta_l)'/f^\beta_l]_{r=S_\beta} \tag{3.5c}$$

is the logarithmic derivative evaluated at the βth muffin-tin sphere boundary, in which f^β_l stands for J^β_l or N^β_l, and f' denotes the radial derivative. In Eq. (3.4), b is the band index, and $\mathbf{k}$ is a two-dimensional wave vector in the two-dimensional Brillouin zone. Then with $\mathbf{r}$ as indicated inside the βth MT sphere, the quantity within large parens in Eq. (3.4) is just the βth MTO, $\chi_{\beta,L}(\mathbf{r})$ of Eq. (3.1) given by the first $\delta_{\alpha\beta}$ term, plus the contribution from the "tails" falling within the βth MT sphere of all other MTO's and of all PWO's. The structure matrix $\Delta^{\beta\alpha}_{L'L}$ is given by

$$\Delta_{L'L}^{\beta\alpha}=\frac{\Phi_{l'}(N_{l'}^{\beta})}{N_{l'}^{\beta}}\frac{\Phi_{l}(N_{l}^{\alpha})}{N_{l}^{\alpha}} \times(B_{L'L}^{\beta\alpha}-e^{i\mathbf{k}\cdot\tau_{\beta\alpha}}\kappa^{l'+l+1}i^{l'-l}T_{L'L}^{\beta\alpha}) , \tag{3.6}$$

where $\tau_{\beta\alpha}=\tau_{\beta}-\tau_{\alpha}$ gives the relative positions of the atoms in the two-dimensional unit cell. The matrices $B_{L'L}^{\beta\alpha}$ and $T_{L'L}^{\beta\alpha}$ are defined in the Appendix of KC. $B_{L'L}^{\beta\alpha}$ is the two-dimensional structure function (in the usual sense of KKR theory), and the matrix $T_{L'L}^{\beta\alpha}$ includes the effects of electronic propagation normal to the film plus a two-dimensional lattice sum of Bessel functions. Thus through $B_{L'L}^{\beta\alpha}$ we include the tails from all the MTO's and through $T_{L'L}^{\beta\alpha}$ we include the tails of all the PWO's. The wave function for the pseudo-muffin-tin sphere is quite similar except now expressions given by (3.3) are used instead of (3.1). A detailed derivation of Eq. (3.4) for the case of a monolayer is given in Appendix B.

The treatment for region III of Fig. 1, i.e., in the "vacuum" above and below the film boundary, is unchanged from KC. We continue to use the tail-cancellation condition in the vacuum region. This means that we restrict the basis function in the vacuum region to the special form given by the solution of the Schrödinger equation for a planar-averaged potential in that region. We now believe that this restriction sufficiently constrains the charge distribution in the boundary region so as to adversely affect the work function. This use of the tail-cancellation condition allows us to specify the coefficients of the PWO's in terms of the coefficients of the MTO's when giving the wave function as a linear combination of MTO's and PWO's. Thus the size of the secular determinant is given by the total number of MTO's assigned to the muffin-tin spheres in the two-dimensional unit cell. Then the wave function in the upper vacuum is

$$\Psi_{\mathbf{k}}^{b}(\mathbf{r}_{\text{upper}})=\sum_{m}A_{1,m}e^{i(\mathbf{k}+\mathbf{g}_m)\cdot\mathbf{r}}u_{\mathbf{k},m}^{(1)}(E_{\text{vac}},z) , \tag{3.7}$$

with a corresponding expression in the lower vacuum. Here E_{vac} is the constant value of energy chosen as representative of the behavior in the vacuum region; $\mathbf{g}_m$ is a two-dimensional reciprocal-lattice vector; $u_{\mathbf{k},m}^{(1)}$ is an exact solution of the one-dimensional Schrödinger equation for a z-dependent potential (z is the direction normal to the film); and the $A_{1,m}^{b}$ are written in terms of the $A_{\alpha,L}^{b}$ (MTO coefficients) using the vacuum tail-cancellation condition.

In the interstitial region the film wave function is

$$\Psi_{\mathbf{k}}(\mathbf{r}_{\text{int}})=\sum_{\alpha,L}A_{\alpha,L}^{b}(\mathbf{k})\sum_{\mathbf{R}}e^{i\mathbf{k}\cdot\mathbf{R}}K_L(\mathbf{r}_{\text{int}}-\mathbf{R}-\tau_{\alpha}) +\sum_{i,m}A_{i,m}^{b}\chi_{i,m}(\mathbf{r}_{\text{int}}) . \tag{3.8}$$

Here $A_{\alpha,L}$ and $A_{i,m}$ have a one-to-one correspondence to the coefficients in Eqs. (3.4) and (3.7). [The index i is 1 (2) for the upper (lower) vacuum.] The $\chi_{i,m}$ are the plane-wave orbitals (PWO's) defined in Eqs. (8a) and (8b) of KC.

C. Wave functions for the linearized augmented muffin-tin orbital method

As was discussed in the Introduction, the work function for the test case (five-layer ⟨100⟩ copper) with fully-warped potential was about 1.5 eV higher than experimental values. This prompted us to explore ways of eliminating the constraint on the vacuum functions so that they were not restricted by the special form of Eq. (3.7). However, since we were reluctant to increase the basis size we did not take the most obvious route of dropping the tail-cancellation condition in the LC(MTO-PWO) method and using the additional variational freedom of the PWO's thus gained. Instead we dropped the PWO's altogether and matched the lattice sum of the muffin-tin orbital tails to a linear combination of $u_{k,m}(E_{\text{vac}},z)$ and $\dot{u}_{k,m}(E_{\text{vac}},z)$ with continuous first derivative at the nominal vacuum boundaries $\pm z_1$. As we shall see in the next section, this actually worsens the results.

For $\mathbf{r}$ in the muffin-tin sphere regions, Eq. (3.4) is valid with the replacement of $T_{L'L}^{\beta\alpha}$ in Eq. (3.6) by

$$D_{L'L}^{\beta\alpha}=\frac{8\pi^2}{A}\frac{i^{l-l'+1}}{\kappa}\sum_{m}-\frac{1}{2Q_m}\{Y_{L'}^{+*}Y_{L}^{+}e^{i\mathbf{g}_m\cdot(\tau_{\beta}-\tau_{\alpha})}[e^{iQ_m(\tau_{\beta}^{z}-\tau_{\alpha}^{z})}+(-1)^{L+L'}e^{-iQ_m(\tau_{\beta}^{z}-\tau_{\alpha}^{z})}]\Theta(Q_m^2)\} , \tag{3.9}$$

where $Y_L^{+}=Y_L(\mathbf{K}_m+Q_m\mathbf{z})$, $\Theta(Q_m^2)$ is the usual unit step function, $Q_m^2=\kappa^2-(\mathbf{k}+\mathbf{g}_m)^2$, and $\mathbf{g}_m$ is the two-dimensional reciprocal-lattice vector. By this replacement we have simply restored the two-dimensional lattice sum of Bessel functions given by (11c) of KC that was included in $T_{L'L}^{\beta\alpha}$. We note for later reference the anti-Hermitean nature of the matrix $D_{L'L}$.

The wave function in the upper vacuum region is

$$\Psi_{\mathbf{k}}^{b}(\mathbf{r})=\sum_{\alpha,L}A_{\alpha,L}^{b}(\mathbf{k})\sum_{m}e^{i\mathbf{K}_m\cdot\mathbf{r}}[F_{\alpha,L;m}^{(1)}u_{\mathbf{k},m}^{(1)}(E_{\text{vac}},z)+G_{\alpha,L;m}^{(1)}\dot{u}_{\mathbf{k},m}^{(1)}(E_{\text{vac}},z)] \tag{3.10}$$

with a corresponding expression for the lower vacuum. $F_{\alpha,L;m}$ and $G_{\alpha,L;m}$ are determined by continuity of the function and derivative across the upper vacuum boundary at $+z_1$, and the other quantities are as defined in Eq. (3.7). We note that Kasowski and Tsai[20] have independently arrived at equations that seem very similar. We use the form given by Eq. (16) of KC for the lattice sum of interstitial functions to carry out the matching at the vacuum boundary. This ensures both accuracy and speed. If Eq. (16) of KC is further expanded in a Fourier series over an interval $\pm z_1$ (as is done to calculate interstitial matrix elements) and that expression used for matching,

as in Eq. (7) of Ref. 20, a large number of plane waves are required in the perpendicular direction to ensure convergence, particularly with terms involving the derivatives. Good convergence is necessary in this case because anti-Hermitean terms arise from matrix elements in the vacuum region that cancel with the anti-Hermitean part that results from Eq. (3.9) when calculating matrix elements from the MT region.

In the interstitial region the film wave function is just Eq. (3.8) with the second term (PWO's) deleted.

D. Poisson equation solution

In this subsection we first discuss the way in which the geometrical problems of solving the Poisson equation are dealt with. We mentioned this problem while presenting the pseudo-muffin-tin wave functions, where we mentioned that having plane wave representations, of both the charge density and the potential, in the interstitial region greatly simplifies the task of solving the Poisson equation. (This is so because the key to solving the Poisson equation lies in defining charge neutral regions of convenient geometrical shape in order to use some version of the Ewald technique for dealing with the lattice of nuclear charges.[26–28])

For purposes of solving the Poisson equation, the two-dimensional unit cell is separated into two regions, each of which is made to be charge neutral. The two regions are the muffin-tin spheres and the entire two-dimensional unit cell. We shall first describe how we obtain a neutral charge distribution in each of these regions, and then how the potential is obtained. For descriptive convenience, we shall describe the procedure as though there were only a single muffin-tin sphere in the two-dimensional unit cell.

We first separate the two-dimensional unit cell into the muffin-tin sphere and the remainder of the cell (interstitial plus vacuum), which for brevity we shall refer to as "interstitial" in the present discussion. We next extend the second region from being the interstitial (i.e., the unit cell with a spherical hole in it) to being the full two-dimensional unit cell. We do this by using the pseudo-muffin-tin wave function defined at the end of Sec. III A. Since this pseudo-muffin-tin wave function is defined so that it is continuous with the true interstitial function, the pseudo-charge density obtained from this is also continuous with the interstitial charge density so that we have a charge density defined over the whole unit-cell region. The pseudo-muffin-tin charge density is now subtracted from region I, the muffin-tin region.

At this point in the procedure for solving the Poisson equation (PE) we have defined two regions, in each of which the PE can be solved separately. These are (1) the muffin-tin sphere and (2) the full unit cell (i.e., unit which repeats periodically in two dimensions). Because of the linearity of the PE, the solution of the PE consists of the sum of the solution in each of the two individual regions. The total charge summed over the two regions is neutral, but each of the regions individually is not charge neutral. To solve the PE in each region, each one must individually be charge neutral. To achieve this we add a Gaussian to the muffin-tin sphere (region 1) and subtract the same Gaussian from the entire unit cell (region 2).

The solution of the PE in regions 1 and 2 is straightforward on taking account of their respective geometries. In region 1, we spherically average the charge; while in region 2, this requires using a Fourier-transformed representation for the charge density (the resulting potential is in the plane-wave form). Calculating the contribution to the Hamiltonian matrix from this Fourier-transformed potential consumes the major fraction of the running time (see Sec. III E for details).

E. Setup of the secular determinant

We now discuss the setting up of the secular determinant which yields the solution of the Schrödinger equation. In doing this we bear in mind that the potential "presented to" the Schrödinger equation is the sum of those in regions 1 and 2 as described above.

The evaluation of the matrix elements of the potential in the muffin-tin sphere is straightforward. The potentials from both regions 1 and 2 contribute to the total potential in the sphere. Except for spherical averaging, we evaluate the matrix elements of the total potential in the sphere exactly.

To evaluate the matrix elements of the potential in the interstitial, we extend the integrals over the potential to the whole unit cell and subtract out a correction for the integral over the muffin-tin sphere, using again the pseudo-muffin-tin functions of Eq. (3.3). In evaluating this correction, we use spherical averaging. Thus whatever warping is present in the pseudo-muffin-tin sphere from the analytic extension of the interstitial charge density is retained in the Hamiltonian. Similarly the overlap matrix from the interstitial region is calculated by first calculating the overlap over the whole unit cell and subtracting from the latter the overlap over the pseudo-muffin-tin region.

Before closing this section a word about Fourier expansions is useful. The interstitial functions, with the help of the pseudo-muffin-tin basis functions, are defined over the whole unit cell. We evaluate and store the corresponding Fourier coefficients. These expansions for both wave function and potential, are over an interval, in the z direction, bounded by $+z_2$ and $-z_2$. These boundaries are approximately one muffin-tin radius outside the nominal vacuum boundaries $+z_1$ and $-z_1$ (see Fig. 1). This achieves the desired accuracy in representing the behavior of the functions at the boundaries $\pm z_1$. The integrals are carried out over the true unit cell defined by the boundaries $\pm z_1$. Integrals involving the potential are currently carried out in configuration space, with the help of FFT, and points in the real-space sum that lie outside the nominal vacuum boundaries are dropped.

IV. QUALITY OF RESULTS AND DISCUSSION

To characterize the quality of results from our two FLMTO methods we consider the following aspects of the output from the calculations. We use results for a five-layer copper $\langle 100 \rangle$ slab as the basis of discussion. First, we exhibit the close agreement of the LC(MTO-PWO) and LAPW eigenvalues for the same input muffin-tin po-

tential, generated from self-consistent atomic charge densities, and the lack of such agreement for the LAMTO method. Second, we report the effect of including various degrees of complexity in the shape approximations used to treat the charge density as input to the Poisson equation and the potential as input to the Schrödinger equation; the discussion will be confined to the LC(MTO-PWO) method. Since we now have the capability of including full warping (except in the muffin tin) in our calculations, the discussion of the shaping approximations is for the sake of completeness and for putting our previously reported calculations[17] in perspective. Third, we report the effect, on the self-consistent results, of varying the energy parameters involved in the linearization. Fourth, and last, we look at the layer-projected density of states and the work functions, comment on the deficiencies, and look at ways to increase the variational freedom in each case.

We test the quality of our LC(MTO-PWO) and LAMTO methods by a preliminary comparison with an accurate LAPW calculation. We use the same film muffin-tin potential, generated from self-consistent atomic charge densities, use the same energy parameters, with suitable choice of κ^2 (within a few millirydbergs of the $E_l=2$ energy parameter, to capture d-band behavior) for both our methods and show the resulting eigenvalues in Table I. The LAPW calculation provides a good standard for comparison because it was done with a large basis that was increased to insure that the calculations were fully converged (i.e., insured that further increase of basis made no difference).

In Table I we have given the energies (in mRy) of the eigenstates classified according to the four symmetry types for the $\mathbf{k}=[(\frac{1}{4},\frac{1}{4})\pi/a]$ point in the two-dimensional Brillouin zone. We see from this table that the LAPW and the LC(MTO-PWO) eigenvalues are in close agreement (differing by 1 or 2 mRy or less in the part of the energy range encompassing the d bands). Thus the LC(MTO-PWO) technique fulfills our expectation of equal variational quality with much greater computational speed (for the film muffin-tin potential). The eigenvalues from the LAMTO method show similar agreement for the $\bar{\Sigma}_2$ and $\bar{\Sigma}_3$ states. The $\bar{\Sigma}_2$ state is pure d while $\bar{\Sigma}_3$ is a mixture of p and d. LAMTO states for the $\bar{\Sigma}_1$ and $\bar{\Sigma}_4$ show the greatest disagreement, ranging from 9—35 mRy, with the corresponding LAPW calculation. The state $\bar{\Sigma}_1$ allows mixing between s, p, and d while $\bar{\Sigma}_4$ has p_z-like states which may hybridize with d's. These differences indicate a problem both in representing states with strong sp-like character and in capturing hybridization effects, as we shall see when examining the self-consistent layer-projected density of states. We recall, in this connection that the Fermi energy of copper is determined by sp-like bands.

We have studied the effect of including various degrees

TABLE I. Comparison of LC(MTO-PWO) and LAMTO eigenvalues with those of LAPW for the same input muffin-tin potential, generated from atomic overlaps, and the same energy parameters (plus specification of κ^2) for both methods described in this paper. For each atom in the unit cell the $l=0$ energy parameters are 540 mRy and for $l=1$ or 2, 420 mRy. The vacuum energy parameter is 420 mRy and κ^2 was set at 449 mRy. A typical point at $\mathbf{k}=(\frac{1}{4},\frac{1}{4})\pi/a$ in the two-dimensional Brillouin zone was chosen for comparison. Eigenvalues are classified by the four symmetry types $\bar{\Sigma}_1$, $\bar{\Sigma}_2$, $\bar{\Sigma}_3$, and $\bar{\Sigma}_4$ for the five-layer ⟨100⟩ copper film.

Energy (mRy), $\bar{\Sigma}_1$ states			Energy (mRy), $\bar{\Sigma}_3$ states		
LAPW	LC(MTO-PWO)	LAMTO	LAPW	LC(MTO-PWO)	LAMTO
−14	20	8	348	349	349
168	193	191	400	402	402
278	302	304	448	448	449
442	443	444	470	471	471
461	462	478	537	538	538
481	482	489			
497	497	506			
511	512	515			
525	526	534			
544	544	552			
655	666	769			

Energy (mRy), $\bar{\Sigma}_2$ states			Energy (mRy), $\bar{\Sigma}_4$ states		
LAPW	LC(MTO-PWO)	LAMTO	LAPW	LC(MTO-PWO)	LAMTO
372	373	373	64	97	121
418	419	419	266	275	335
448	448	449	430	431	448
504	505	506	451	452	456
556	556	556	480	481	489
			488	488	497
			503	504	538
			537	537	552

of complexity in the shape approximations used to treat the charge density as input to the Poisson equation and the potential as input to the Schrödinger equation for the LC(MTO-PWO) method. We only briefly discuss this study because we now have the capability to routinely include full warping for the potential in our calculations. However, we note that substantial amounts of running time may be saved if for some purposes it is felt that including vertical warping in the potential is sufficient.

The first shaping approximation consisted of averaging the charge density, spherically in the muffin-tins, over the volume in the interstitial, and over planes parallel to the film in the vacuum *before* solving the Poisson equation for each iteration. The resulting self-consistent work function of 10 eV for five-layer ⟨100⟩ copper is much too large compared to an experimental value[29–31] of 4.6–4.8 eV. The potential for each iteration in this case is the film muffin-tin potential.

As the second shaping approximation we still use the film muffin-tin potential at each iteration for solving the Schrödinger equation but the charge density input to the Poisson equation was allowed full spatial variation in all regions except the muffin-tin sphere where it was spherically averaged. The resulting potential was shaped to film muffin-tin form. The self-consistent work function was better at 8 eV, but still too large.

As the next shaping approximation in solving the Schrödinger equation, we include vertical warping in the interstitital potential. We then obtain a work function of 4.9 eV in excellent agreement with experiment, as well as agreeing very closely with previous self-consistent calculations[21,22] for ⟨100⟩ copper. (We mention that the vertically-warped results were also excellent for ⟨100⟩ five-layer nickel, but the work function for ⟨0001⟩ ruthenium was too small by about 1 eV.) There is some ambiguity in the definition of planar averaging and we now discuss this in greater detail along with our procedure for handling the exchange and correlation for this case, so that our results with full warping (except in the muffin tin) of the potential (to be presented at the end of the discussion) can be put in perspective.

For simplicity of discussion it is useful to start with a potential that is allowed full spatial variation in the interstitial region. We recall that by the process of analytic continuation of the wave function, and hence the charge density, the interstitial potential is extended over the whole unit cell. We further recall that the muffin-tin zero is defined[5] as the *interstitial average* of the potential. The process of interstitial averaging may be imagined as first planar averaging over planes parallel to the film boundary but with circular holes cut out of them, corresponding to planes of intersection with the muffin-tin spheres. This planar-averaged potential must now be averaged in the perpendicular direction between the nominal vacuum boundaries at $\pm z_1$, to give the muffin-tin zero of the potential. The same result may be achieved by convoluting the unit-cell potential with a three-dimensional step function that takes the value zero within the muffin-tin sphere regions. However, a large number of Fourier coefficients of the potential must be kept to represent the sharp falloff of the step at the muffin-tin sphere boundary. To save computer time we have resorted to a cruder approach. We simply planar averaged (right through the muffin-tin spheres) the unit-cell potential (i.e., over the complete plane regardless of whether it cut through a muffin-tin sphere region). The resulting planar-averaged potential is in error from contributions of the analytic extension of the potential into the muffin-tin regions. If this planar-averaged potential is now averaged in the perpendicular direction, the result is not the muffin-tin zero. We corrected for this by subtracting a constant (recalculated at each iteration) equal to the difference between the muffin-tin zero and the average value of the crude planar-averaged potential (i.e., the average over the whole unit cell). This constant, which we expected to be small, is surprisingly large, being about -500 mRy. A second error is introduced by our handling of the exchange and correlation which is calculated using a charge density that is shaped to the same form (i.e., vertically warped, planar averaged in vacuum) as the final potential that is used in the crystal Schrödinger equation. This then is the vertically-warped potential that we used in reporting our earlier results.[17]

We have now implemented the fast Fourier transform, and routinely use potentials of full spatial variation in the interstitial and vacuum and charge density of full spatial variation (spherically averaged in MT sphere region) in calculating the exchange correlation contribution. This avoids the errors mentioned above. The resulting self-consistent work function with the LC(MTO-PWO) method for five-layer ⟨100⟩ copper is 6.3 eV (compared to the experimental value[29–31] of 4.6–4.8 eV).

To study the effect of varying the energy parameters involved in the linearization on the energy eigenvalues and

TABLE II. Fermi energy and work function for several sets of energy parameters. (Calculations were for five-layer ⟨100⟩ copper.) Energies are in mRy except for work functions, which are in eV. The first three sets are for the LC(MTO-PWO) method, with vertical warping for the first two and full warping for the third as explained in the text. The last two sets are with the LAMTO method with fully-warped potential.

Set	$E_{l=0}$	$E_{l=1}$	$E_{l=2}$	E_{vac}	κ^2	E_F	Φ
1	150	200	290	400	90	503	4.4
2	150	200	290	400	292	480	4.9
3	150	150	290	450	292	464	6.3
4	150	150	350	510	397	521	6.9
5	150	150	350	510	490	534	6.4

TABLE III. Energy eigenvalues at $\mathbf{k}=(\frac{1}{4},\frac{1}{4})\pi/a$ for first three sets of energy parameters shown in Table II. Energies are in mRy.

Set 1	Set 2	Difference (1−2)	Set 3	Set 1	Set 2	Difference (1−2)	Set 3
−126	−130	4	−108	355	329	26	321
−45	−51	6	−24	366	338	28	329
59	50	9	94	370	342	28	334
132	115	17	174	380	351	29	335
141	120	21	177	383	354	29	344
216	192	24	196	386	356	30	345
238	212	26	218	390	362	28	353
267	239	28	246	402	370	32	365
291	263	28	262	403	372	31	373
310	282	28	286	411	383	28	376
327	300	27	288	416	384	32	376
330	305	25	291	430	401	29	390
333	308	25	294	435	410	25	392
344	318	26	294	511	491	20	447
352	325	27	311				

work function, we have studied shifts in behavior between results for different sets of energy parameters. We present these results in Table II. Two sets are shown for the LC(MTO-PWO) method with vertical warping, one set (set 3) with full warping, and sets 4 and 5 are for the LAMTO with full warping. The table displays only variations with respect to κ^2 between sets 1 and 2 and between sets 4 and 5, because the methods seem to be the most sensitive to that parameter. In the following discussion we shall make use of results that are not explicitly given in the table. Comparing sets 1 and 2 we see that the rather large change in κ^2 brings about a significant but smaller change in the work function (of about 0.5 eV), while the shift in energy eigenvalues is rigid (i.e., constant) within 30 mRy or less over most of the energy range (see Table III). This change in κ^2 required about eight iterations for reconvergence of the potential to within 10 mRy; smaller changes in κ^2 require fewer iterations. The method is least sensitive to the $l=0,1$, and vacuum energy parameters and somewhat more sensitive to the $l=2$ energy parameter, requiring between four and eight iterations for reconvergence for variations between 90 and 490 mRy. The corresponding largest shift in the work function is only 0.2 eV. In Table III we also show a set of eigenvalues for the fully-warped calculation with the LC(MTO-PWO) method (set 3) for comparison; the shift in the eigenvalues from those of set 2 is less than 20 mRy over most of the energy range, with little spectral distortion, while the work function moves up significantly to 6.3 eV.

The LAMTO method (sets 4 and 5, Table II) shows greater sensitivity to changes in κ^2 (changes of about 100 mRy shifting the work function by 0.5 eV). Set 4 corresponds to a "reasonable" choice of κ^2 (i.e., close to the position of d bands). As many as 12 iterations may be required with the LAMTO for reconvergence to within 10 mRy for the potential. The work function is no better than that with the LC(MTO-PWO) method (however, see 23), and, as we shall see, the corresponding layer-projected density of states is very poor.

We now discuss our layer-projected density of states for five-layer ⟨100⟩ Cu shown in Figs. 2–4. The first two figures are with the LC(MTO-PWO) method for the vertically- and fully-warped potentials, respectively, and the third is with the LAMTO method using the fully-warped potential. In each case the top panel is the surface

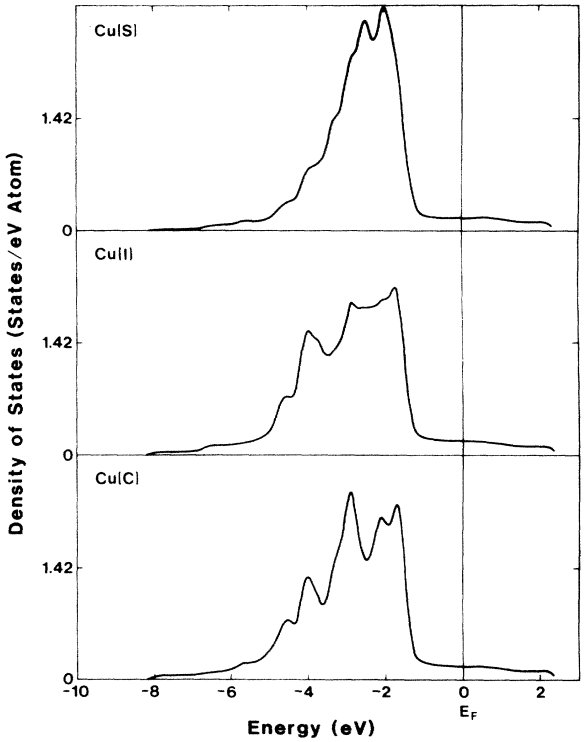

FIG. 2. Layer-projected density of states for a system consisting of a five-layer slab of (100) Cu. *S*, *I*, and *C* denote the surface, interface (next-to-surface), and center layers, respectively. This calculation is for a vertically-warped potential using the LC(MTO-PWO) method as described in the text. The density of states should be multiplied by 2 to take account of spin degeneracy.

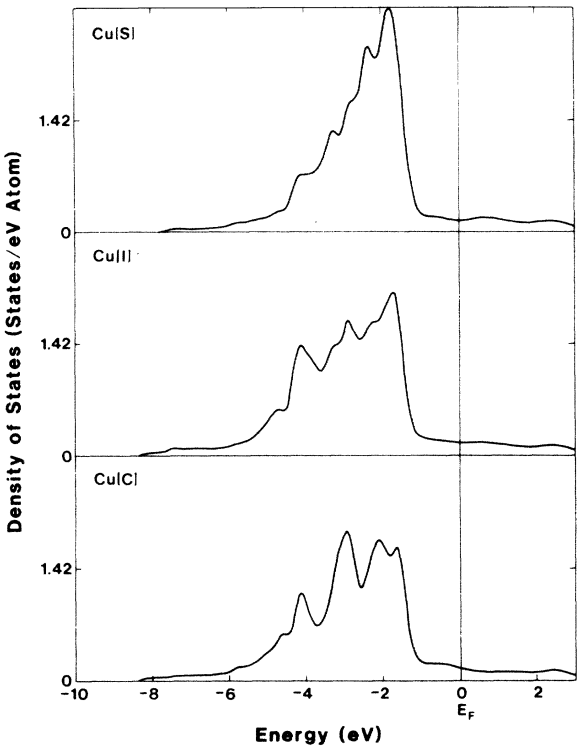

FIG. 3. Layer-projected density of states for a system consisting of a five-layer slab of (100) Cu. *S*, *I*, and *C* denote the surface, interface (next-to-surface), and center layers, respectively. This calculation is for a fully-warped potential using the LC(MTO-PWO) method as described in the text. The density of states should be multiplied by 2 to take account of spin degeneracy.

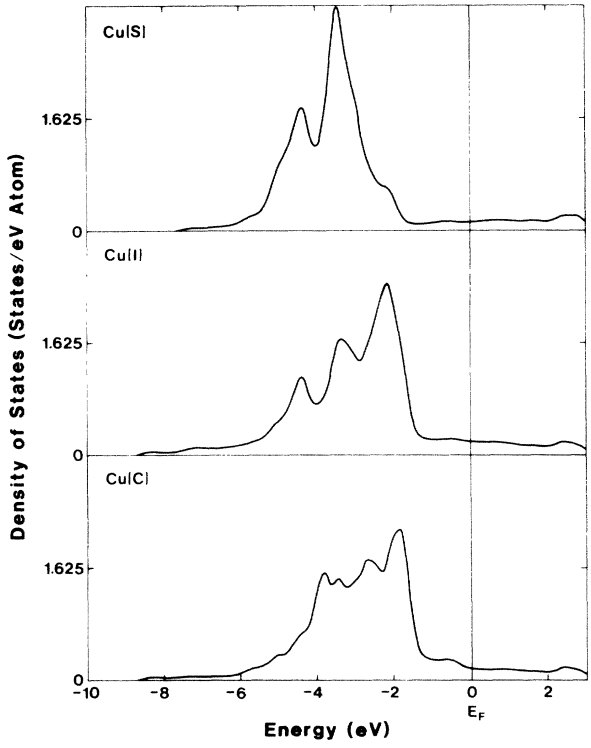

FIG. 4. Layer-projected density of states for a system consisting of a five-layer slab of (100) Cu. *S*, *I*, and *C* denote the surface, interface (next-to-surface), and center layers, respectively. This calculation is for a fully-warped potential using the LAMTO method as described in the text. The density of states should be multiplied by 2 to take account of spin degeneracy.

layer, the middle panel is the subsurface layer, and the bottom panel is the center layer. For both methods there is very little (barely noticeable) change in spectral shape with changes in energy parameters. Upon comparing Figs. 2 and 3 we see that in the surface layer the leading edge shows a small shift of about a tenth of an eV. There are some minor changes in the shape for all three layers. As far as we can judge, the layer density of states with either vertically or fully-warped potential for the LC(MTO-PWO) method shows good agreement with other self-consistent calculations.[21] The density of states with the LAMTO method, on the other hand, shows serious distortions for the surface layer (Fig. 4, top panel). The start of the initial rise is about an eV lower, and while the LC(MTO-PWO) method gives a peak within half an eV from the initial rise, the rise for the LAMTO calculation continues over 1.8 eV from its onset before reaching its maximum. Further, it does not exhibit the series of steps on its trailing edge. The density of states are shifted half an eV downward for the subsurface and center layers from those of the LC(MTO-PWO) method.

We now present qualitative arguments for each method to show that the variational freedom must be increased to obtain good work functions, while retaining a good-quality layer-projected density of states for the LC(MTO-PWO) method. In the LC(MTO-PWO) method, even with the use of the tail-cancellation condition in the vacuum, the basis functions are a mixture of MTO's and PWO's that provide a good representation to capture all the essential features of the layer-projected density of states. However, the constraint on the vacuum functions limits the variational freedom of the method and the ability of the charge to readjust near the vacuum boundary, giving a poor value of the work function. In Appendix A we suggest a way of utilizing the full power of the LC(MTO-PWO) method and avoiding the convergence problems[5] in the exterior regions. This we believe will give us good work functions, in addition to the already good layer density of states with only a modest increase in the size of the secular determinant, thus still providing computational advantages for studying complex systems with many atoms in the unit cell.

We recall, as was described in the Methodology section, that if we take the LC(MTO-PWO) method *without* imposing the tail-cancellation condition, delete the PWO's everywhere, and replace the lattice sum of MTO tails in the vacuum by a linear combination of $u_m(z)$ and $\dot{u}_m(z)$ with continuous logarithmic derivative at the vacuum boundary, we get the LAMTO method. However, deleting the PWO's renders the resulting formalism, in the exact limit, inequivalent to the film KKR method due to loss of scattering information from the vacuum boun-

daries. In practice, as we see from the results, the LAMTO method is inferior (as it stands) to the LC(MTO-PWO) method with the same size basis. We believe that this occurs for two reasons, which may be related and equally important. First, the basis functions in the vacuum exhibit broad peaks outside the nominal boundary region for $l=0$ and 1. This is unlike the functions for the LC(MTO-PWO) method which exhibit exponentially decaying behavior. If we think of the interstitial and vacuum potential as being qualitatively similar to an ideal square-well potential in the z direction, it is clear that the latter functions are the better representation. Second, the absence of PWO's in the muffin-tin and interstitial regions may represent an important handicap in capturing hybridization effects and the position of the s- and p-like bands near the Fermi energy for the copper system. This is because a relatively few LMTO's alone may be inadequate to capture the necessary behavior in the perpendicular direction within the interstitial region. We contrast this behavior with the bulk systems where periodicity in all three directions enables the use of modulated plane waves in all three directions in the bulk LMTO method. Thus the absence of PWO's means that a substantial expansion in the number of basis functions may be needed to improve the LAMTO method. In our future work we plane to revert to the LC(MTO-PWO) method.

V. SUMMARY AND CONCLUSIONS

In our efforts to adapt the LMTO method to slab geometries we have explored the use of two modifications of MTO basis functions as used in bulk calculations, with the object of minimizing demands on computer resources without sacrificing quality of results. Of these two versions of the LMTO method for slabs, on the basis of the detailed study described above, the LC(MTO-PWO) method incorporating the tail-cancellation method is much more promising. This method gives good, and we believe adequate, spectra of eigenvalues for understanding the electronic behavior of surfaces insofar as these are characterized by the layer-projected density of states, but gives generally inadequate work-function values. We believe that this defect with regard to the work-function values is a consequence of the constraint placed on the charge distribution in the vacuum boundary region through use of the tail-cancellation constraint in defining the basis functions. Therefore, in Appendix A we have outlined the modifications in the LC(MTO-PWO) method necessary upon eliminating the tail-cancellation constraint.

The question of whether the work function is a good "one-number" test of self-consistent electronic structure calculations, along with the effects of use of various exchange-correlation potentials, has been discussed in detail by Jepsen and Wilkins[11] for the LAPW method. (We do not expect the answer to be different for the LMTO method.) It is possible to have the correct relative energy distribution of states, but a poor work function, because the latter depends on the correct positioning of the Fermi energy with respect to the absolute zero of potential at infinity (vacuum zero). Thus a rigid shift of the bands would not affect the density of states, and yet would give a poor work function.

The second version of the LMTO method we have explored for slab geometries, the LAMTO method, does poorly both for the work function and for the density of states, because discarding the PWO's worsens the quality of the basis functions even in the muffin-tin regions. We have now implemented and tested the third method, the LC(MTO-PWO) method, without tail cancellation, suggested in Appendix A. The results have fulfilled our expectations and will be reported elsewhere.[32]

We have also investigated the sensitivity of the eigenvalues with respect to changes in the energy parameters and the effect on the work function of various shaping approximations of the charge density distribution and potential. The eigenvalues are stable with respect to changes in the energy parameters. Averaging the charge density outside the muffin-tin spheres before calculating the potential strongly affects the work function, while averaging the potential (as calculated from the charge density with complete spatial variation) has a much smaller effect.

ACKNOWLEDGMENTS

The research at West Virginia University has been supported by the U. S. Department of Energy and the West Virginia University Energy Research Center. The research at the College of William and Mary has been supported by National Science Foundation Grant No. DMR-84-16046. We are grateful for valuable discussions with Dr. John M. Wills.

APPENDIX A

In Appendix A, we increase the variational freedom for the LC(MTO-PWO) method by making the PWO's independent functions. We restrict our attention to the upper vacuum $z \geq z_1$, since the lower vacuum can be dealt with similarly. Using the expression given by the left side of Eq. (15a) of KC for the crystal wave function for r in the upper vacuum, and making use of Eq. (16) of KC to rewrite that, we have

$$\sum_m e^{i\mathbf{K}_m\cdot\mathbf{r}}\left[\left[\frac{2\pi i}{A}\sum_{\alpha,L}A_{\alpha,L}(\mathbf{k})\frac{\kappa^l Y_L^+}{Q_m}e^{-i\mathbf{K}_m\cdot\tau_\alpha - iQ_m\tau_{\alpha_z}}+A_{1,m}c_{1,m}+A_{2,m}s_{2,m}\right]e^{iQ_m z}+A_{1,m}u^{(1)}_{\mathbf{k},m}(z)\right]. \tag{A1}$$

As noted in Sec. IV of KC, for $Q_m^2>0$, the integrals (for calculating matrix elements of the secular determinant) in the vacuum regions do not converge. This problem can be circumvented in the same way that false zeros due to nonorthogonality of the MTO tails were eliminated. This is accomplished by replacing the oscillating function $e^{iQ_m z}$ with a linear combination of $u^{(1)}_{\mathbf{k},m}(z)$ and its energy derivative matched with continuous first derivative at the vacuum boundary. This linear combination takes the form

$$e^{iQ_m z}\rightarrow -2iQ_m[\dot{s}_{1,m}u^{(1)}_{\mathbf{k},m}(z)-s_{1,m}\dot{u}^{(1)}_{\mathbf{k},m}(z)],\quad z>z_1\ , \tag{A2}$$

where $s_{1,m}$ is as defined in KC and $\dot{s}_{1,m}$ is its energy derivative. This replacement is strictly not necessary for $Q_m^2<0$. However, numerical integrations involving the product of $u^{(1)}_{\mathbf{k},m}(z)$ and $e^{-Q_m z}$ may be avoided if the replacement (A2) is made for all values of Q_m^2.

The wave function in the interstitial region is still given by Eq. (3.8), but the $A^b_{i,m}$ are now independent variational coefficients. In the muffin-tin region the wave function is

$$\Psi^b_{\mathbf{k}}(\mathbf{r})=\sum_{\alpha,L}A^b_{\alpha,L}(\mathbf{k})\left[\Phi_L(N^\alpha_l,\mathbf{r}')\delta_{\alpha\beta}+\sum_{L'}\frac{\Phi_{L'}(J^\beta_{l'},\mathbf{r}')}{\omega_{l'}(N^\beta_{l'})-\omega_{l'}(J^\beta_{l'})}\Delta^{\beta\alpha}_{L'L}\right]+\sum_{i,m}A^b_{i,m}\chi_{i,m}(\mathbf{r})\ , \tag{A3}$$

$\mathbf{r}\in$ the βth MT sphere where $\mathbf{r}'=(\mathbf{r}-\tau_\beta)$, and where $\Delta^{\beta\alpha}_{L'L}$ is now given by Eq. (2.6) with $T^{\beta\alpha}_{L'L}$ replaced by $D^{\beta\alpha}_{L'L}$ of Eq. (3.9). The $\chi_{i,m}(\mathbf{r})$ are the plane-wave tails from the two vacuum regions of the form $e^{i\mathbf{K}_m\cdot\mathbf{r}\pm iQ_m z}$ which must now be expanded in spherical waves inside the muffin-tin with the Bessel function in the expansion replaced by the appropriate linear combination of $u_{\beta,l}$ and $\dot{u}_{\beta,l}$.

APPENDIX B

In Appendix B we present the derivation of the representation of the linearized film wave function for $\mathbf{r}$ within the muffin-tin sphere for the case of a monolayer film [derivation of Eq. (3.4) for the monolayer case]. From Eq. (9) of KC, the wave function for $|\mathbf{r}|\le S$ (within the muffin-tin sphere) is

$$\Psi_{\mathbf{k}}(\mathbf{r})=\sum_L A_L(\mathbf{k})\sum_{\mathbf{R}}e^{i\mathbf{K}\cdot\mathbf{R}}\chi_L(\mathbf{r}-\mathbf{R})+\sum_{i,m}A_{i,m}(\mathbf{k})\chi_{i,m}(\mathbf{r})\ . \tag{B1}$$

Using the explicit expression for the MTO, $\chi_L(\mathbf{r}-\mathbf{R})$, as given by Eq. (4a) of KC, we have

$$\Psi_{\mathbf{k}}(\mathbf{r})=\sum_L A_L[u_L(\mathbf{r})+(c_l+is_l\kappa^{2l+1})J_L(\mathbf{r})]+\sum_L A_L\sum_{\mathbf{R}(\neq 0)}e^{i\mathbf{k}\cdot\mathbf{R}}s_l K_L(\mathbf{r}-\mathbf{R})+\sum_{i,m}A_{i,m}\chi_{i,m}(\mathbf{r})\ . \tag{B2}$$

It can be shown that

$$\sum_L A_L\sum_{\mathbf{R}(\neq 0)}e^{i\mathbf{k}\cdot\mathbf{R}}s_l K_L(\mathbf{r}-\mathbf{R})+\sum_{i,m}A_{i,m}\chi_{i,m}(\mathbf{r})=-\sum_L A_L s_l[i\kappa^{2l+1}J_L(\mathbf{r})]+\sum_L A_L s_l\sum_{L'}J_{L'}(\mathbf{r})[B_{L'L}-i^{l'-l}\kappa^{l'+l+1}T_{L'L}],\quad \text{for } \kappa^2>0\ . \tag{B3}$$

Therefore,

$$\Psi_{\mathbf{k}}(\mathbf{r})=\sum_L A_L[u_L(\mathbf{r})+c_l J_L(\mathbf{r})]+\sum_L A_L s_l\sum_{L'}J_{L'}(\mathbf{r})(B_{L'L}-i^{l'-l}\kappa^{l'+l+1}T_{L'L})\ . \tag{B4}$$

Linearization implies that

$$u_L(\mathbf{r})+c_l J_L(\mathbf{r})=s_l\dot{c}_l\Phi_L(N_l,\mathbf{r})\ , \tag{B5a}$$

$$J_{L'}(\mathbf{r})=\dot{s}_{l'}\Phi_L(J_l,\mathbf{r})\ , \tag{B5b}$$

where $\dot{c}_l$ and $\dot{s}_l$ are the energy derivatives of the coefficients c_l and s_l, respectively.

The wave function can now be written as

$$\Psi_{\mathbf{k}}(\mathbf{r})=\sum_L A_L s_l\dot{c}_l\left[\Phi_L(N_l,\mathbf{r})+\sum_{L'}\frac{\dot{s}_{l'}}{\dot{c}_l}\Phi_{L'}(J_l,\mathbf{r})(B_{L'L}-i^{l'-l}\kappa^{l'+l+1}T_{L'L})\right]\ . \tag{B6}$$

Redefine $A_L s_l \dot{c}_l \equiv A_l$; and from the boundary conditions at the MT radius we get that

$$\frac{\dot{s}_{l'}}{\dot{c}_l} = \frac{\Phi_{l'}(N_{l'})}{N_{l'}} \frac{\Phi_l(N_l)}{N_l} \frac{1}{\omega_{l'}(N_{l'}) - \omega_{l'}(J_{l'})} . \tag{B7}$$

Hence

$$\Psi_{\mathbf{k}}(\mathbf{r}) = \sum_L A_L(\mathbf{k}) \left[\Phi_L(N_l, \mathbf{r}) + \sum_{L'} \frac{\Phi_{L'}(J_{l'}, \mathbf{r})}{\omega_{l'}(N_{l'}) - \omega_{l'}(J_{l'})} \Delta_{L'L} \right] , \tag{B8}$$

with

$$\Delta_{L'L} \equiv \frac{\Phi_{l'}(N_{l'})}{N_{l'}} \frac{\Phi_l(N_l)}{N_l} (B_{L'L} - i^{l'-l} \kappa^{l'+l+1} T_{L'L}) . \tag{B9}$$

---

*Present address: AT&T Bell Laboratories, Allentown, PA 18103.

†Present address: NASA Langley Research Center, Hampton, VA 23665.

[1]O. Jepsen, J. Madsen, and O. K. Andersen, Phys. Rev. B **18**, 605 (1978).

[2]H. Krakauer, M. Posternak, and A. J. Freeman, Phys. Rev. B **19**, 1706 (1979).

[3]E. Wimmer, A. J. Freeman, M. Weinert, H. Krakauer, J. R. Hiskes, and A. M. Karo, Phys. Rev. Lett. **48**, 1128 (1982).

[4]P. J. Feibelman, J. A. Appelbaum, and D. R. Hamann, Phys. Rev. B **20**, 1433 (1979).

[5]H. Krakauer and B. R. Cooper, Phys. Rev. B **16**, 605 (1977).

[6]C. Q. Ma, H. Krakauer, and B. R. Cooper, J. Vac. Sci. Technol. **18**, 581 (1981).

[7]L. Richter, S. D. Bader, and M. B. Brodsky, J. Vac. Sci. Technol. **18**, 578 (1981).

[8]O. K. Andersen, Phys. Rev. B **12**, 3060 (1975).

[9]O. Jepsen, O. K. Andersen, and A. R. Mackintosh, Phys. Rev. B **12**, 3084 (1975).

[10]T. Jarlborg, A. J. Freeman, and T. Watson-Yang, Phys. Rev. Lett. **39**, 1032 (1977).

[11]O. Jepsen and J. W. Wilkins (unpublished).

[12]J. W. Davenport, Phys. Rev. B **29**, 2896 (1984).

[13]D. R. Hamann, Phys. Rev. Lett. **46**, 1227 (1981).

[14]P. Hohenberg and W. Kohn, Phys. Rev. **136**, B864 (1964); W. Kohn and L. J. Sham, *ibid.* **140**, A1133 (1965).

[15]E. Wigner, Phys. Rev. **46**, 1002 (1934).

[16]For example, see B. Segall and F. S. Ham in *Methods in Computational Physics*, edited by B. Alder, S. Fernbach, and M. Rotenberg (Academic, New York, 1968), Vol. 8, Chap. 7.

[17]C. Q. Ma, M. V. Ramana, B. R. Cooper, and H. Krakauer, J. Vac. Sci. Technol. A **1**, 1095 (1983).

[18]F. J. Himpsel, K. Christmann, P. Heimann, and D. E. Eastman, Phys. Rev. B **23**, 2548 (1981).

[19]M. V. Ramana, B. R. Cooper, H. Krakauer, and C. Q. Ma, Bull. Am. Phys. Soc. **29**, 265 (1984).

[20]R. V. Kasowski and M.-H. Tsai, Phys. Rev. B **29**, 1043 (1984).

[21]J. R. Smith, J. G. Gay, and F. J. Arlinghaus, Phys. Rev. B **21**, 2201 (1980).

[22]A. Euceda, D. M. Bylander, L. Kleinman, and K. Mednick, Phys. Rev. B **27**, 659 (1983).

[23]We note that for the LAMTO method described in the text we have used Hankel functions in the interstitial. This choice is not unique, and for $\kappa^2 > 0$ we have run a parallel calculation with Neumann functions in the interstitial, obtained from Eqs. (2) of KC by adding the appropriate solution of the homogeneous equation. The resulting MTO's are not normalizable for $\kappa^2 < 0$, and the resulting wave functions are not equivalent to those obtained with Hankel functions in the interstitial. This is unlike the three-dimensional case where the lattice sum over Bessel functions is zero. The resulting work function varies over about 2 eV with changes in κ^2 with no improvement in the layer density of states compared to those obtained with Hankel functions in the interstitial. The range of variation of the work function included the experimental value for a value of κ^2 close to the center of the d bands. Thus it is possible to get a good work function and yet have layer density of states that are poor.

[24]C. S. Wang and A. J. Freeman, Phys. Rev. B **19**, 793 (1979).

[25]See Appendix A of Ref. 2.

[26]P. P. Ewald, Ann. Phys. **64**, 253 (1921).

[27]J. C. Slater and P. DeCicco, MIT Solid State and Molecular Theory Group Quarterly Progress Report No. 50, 1963 (unpublished), p. 46.

[28]W. A. Harrison, *Pseudopotentials in the Theory of Metals* (Benjamin, New York, 1966), Chap. 5, p. 165 *et seq.*

[29]P. O. Gartland, S. Berge, and B. J. Slagsvold, Phys. Rev. Lett. **28**, 738 (1972).

[30]G. A. Haas and R. E. Thomas, J. Appl. Phys. **48**, 86 (1977).

[31]G. C. Tibbetts, J. M. Burkstrand, and J. C. Tracy, Phys. Rev. B **15**, 3652 (1977).

[32]G. W. Fernando, B. R. Cooper, M. V. Ramana, H. Krakauer, and C. Q. Ma, Phys. Rev. Lett. **56**, 2299 (1986).